Paleomagnetism from Deception Island (South Shetlands archipelago, Antarctica), new insights into the interpretation of the volcanic evolution using a geomagnetic model

B. Oliva-Urcia1 · I. Gil-Pena2 · A. Maestro1,2 · J. Lopez-Martinez1 · J. Galindo-Zaldivar3,4 · R. Soto5 · A. Gil-Imaz6 · J. Rey7 · O. Pueyo6

B. Oliva-Urcia
belen.oliva@uam.es
I. Gil-Pena
i.gil@igme.es
A. Maestro
a.maestro@igme.es
J. Lopez-Martinez
jeronimo.lopez@uam.es
J. Galindo-Zaldivar
jgalindo@ugr.es
R. Soto
r.soto@igme.es
A. Gil-Imaz
agil@unizar.es
J. Rey
jjrey@esgemar.com

1. Departamento de Geología y Geoquímica, Facultad de Ciencias, Universidad Autónoma de Madrid, 28049 Madrid, Spain
2 Instituto Geológico y Minero de España, Ríos Rosas, 23, 28003 Madrid, Spain
3 Departamento de Geodinámica, Universidad de Granada, 18071 Granada, Spain
4 Instituto Andaluz de Ciencias de la Tierra, 18071 Granada, Spain
5 Instituto Geológico y Minero de España, Unidad de Zaragoza, Manuel Lasala, 44-9 • ‹B, 50006 Zaragoza, Spain
6 Área de Geodinámica Interna, Departamento de Geología, Universidad de Zaragoza, 50009 Zaragoza, Spain
7 ESGEMAR, Espacio 4, Polígono San Luís, 29006 Málaga, Spain

Abstract Deception Island shows the most recent exposed active volcanism in the northern boundary of the Bransfield Trough. The succession of the volcanic sequence in the island is broadly divided into pre- and post-caldera collapse units although a well-constrained chronological identification of the well-defined successive volcanic episodes is still needed. A new paleomagnetic investigation was carried out on 157 samples grouped in 20 sites from the volcanic deposits of Deception Island (South Shetlands archipelago, Antarctic Peninsula region) distributed in: (1) volcanic breccia (3 sites) and lavas (2 sites) prior to the

caldera collapse; (2) lavas emplaced after the caldera collapse (10 sites); and (3) dikes cutting pre- and the lowermost post-caldera collapse units (5 sites). The information revealed by paleomagnetism provides new data about the evolution of the multi-episodic volcanic edifice of this Quaternary volcano, suggesting that the present-day position of the volcanic materials is close to their original emplacement position. The new data have been combined with previous paleomagnetic results in order to tentatively propose an age when comparing the paleomagnetic data with a global geomagnetic model. Despite the uncertainties in the use of averaged paleomagnetic data per volcanic units, the new data in combination with tephra occurrences noted elsewhere in the region suggest that the pre-caldera units (F1 and F2) erupted before 12,000 year BC, the caldera collapse took place at about 8300 year BC, and post-caldera units S1 and S2 are younger than 2000 year BC.

Introduction

he most common methods used for dating volcanic rocks are radiometric, especially potassium–argon (K/Ar), argon–argon (40Ar/39Ar), uranium–lead (Pb/U) and radiocarbon dating (14C). Nevertheless, in many situations radiometric dating is not possible, or difficult: in case of evident post-depositional alteration, or when the minerals content is not suitable (e.g., low K-content), or in case of rocks too young to show isotopic decay. Both 40Ar/39Ar and K/Ar methods can lose accuracy in young (Holocene) and less evolved products, especially in K-poor volcanic rocks (i.e., basalts erupted in most intra-oceanic volcanoes). 14C is a powerful dating tool for dating last millennia, and indeed, it is the most suitable and commonly used for Holocene sediments, but organic material or soils are required, which can be absent in many cases in Antarctic environments.

An additional complication for 14C dating of volcanic events in the Antarctic is the uncertainty over radiocarbon reservoir effects in that region which yielded older than expected ages in lake and marine sediments (Björck et al. 1991a, b; Ingólfsson et al. 1992; Hjort et al. 1997; Takahashi et al. 1999; Hall and Henderson 2001). Moreover, when dealing with volcanic environments, in some cases soils or lahars can also bear organic materials, which form at favorable climatic conditions and when the eruption rate is low enough for a soil to develop. Therefore, in the case of active volcanoes with high frequency of eruptions, soils cannot form and the 14C method cannot be used. When radiometric dating is not possible, variations in the geomagnetic field recorded in volcanic rocks can be used as a dating tool for eruptions. The advantage of the paleomagnetic dating method is that it can be used on wholerock samples and does not need particular petrographic/ chemical characteristics (magnetic remanence is generally carried by titanomagnetite series of minerals, ubiquitous in volcanic rocks). The reliability of paleomagnetic dating depends on the availability of geomagnetic models and on the accuracy of paleomagnetic determinations in the región under investigation.

Deception Island, South Shetland Islands, off the northern Antarctic Peninsula is a Quaternary volcano with an inner bay (Port Foster), which shows the most recent activity in the Bransfield Strait region (e.g., Baker et al. 1975).

The products of numerous eruptions have been recorded as a result of detailed mapping (e.g., Smellie 2002). Although their relative ages are well defined, their absolute chronological ages are not and only the ages of a few historical eruptions are known (Smellie 2002). The remainder of the island lacks a chronology and, in particular, the age of the major caldera-forming eruption, which is the most important eruptive episode to have occurred, is unknown (Smellie et al. 1984; Smellie 2002; Martí et al. 2013). The island is a shield volcano, with a submerged basal diameter of about 30 km and a summit at Mount Pond (540 m), which rises ~1.5 km from the sea floor (Smellie 1990). The current morphology of the island shows a central flooded caldera and a variety of craters, lavas and different volcanic deposits (e.g., tephra, tuffs, scoria) partially covered by ice (López-Martínez et al. 2000). Classically, authors who have studied the volcanic sequences in Deception Island determined a caldera collapse, which allows separating the volcanic deposits in pre- (or pre- and syn-) and post-caldera collapse (e.g., Hawkes 1961; Baker et al. 1975; Birkenmajer 1992; Smellie and López-Martínez 2000; Martí et al.2013). The pre-caldera deposits include the Port Foster Group (F1, F2 and F3 formations in this work), and the post-caldera deposits include the Mount Pond Group (S1 and S2) (following Smellie and López-Martínez 2000). The collapse was considered to be caused by concentric faults (Hawkes 1961; Baker et al. 1975; Birkenmajer 1992) although more recent geophysical studies have shown that the gravimetric and magnetic anomalies are not related to a typical circular structure of a classic volcanic caldera but rather reveal a NE–SW linear trend in the crustal mass (Ortiz et al. 1992; Funaki et al. 2012; Martí et al. 2013).

A large eruption is likely related to the caldera collapse, although the collapse would have exploited any preexisting tectonic features (Smellie 2002). The main objective of this paper is to constrain relative ages of the different igneous rock units after comparing the averaged paleomagnetic data per unit to global geomagnetic models (Pavón-Carrasco et al. 2014) once we decipher whether the present-day positioning of the volcanic deposits of Deception Island (lavas, pillow lavas with scoria, and pyroclastic lavas) is original or other post-cooling processes [tectonic deformation or tilting due to the evolution of the volcanic edifice after the thermoremanent magnetization (TRM) acquisition] have modified the attitude of the volcanic deposits to their present position using paleomagnetic data. This study has been carried out by combining 20 new sampling sites from Deception Island rocks with previous data from Baraldo et al. (2003) (17 sites).

Geological setting, studied material and previous paleomagnetic data

Deception Island is located in the boundary between the South Shetland crustal block and the southwestern part of the Bransfield Trough, a young (<1.4 Myr), narrow, elongated, ENE–WSW basin located between the South Shetlands archipelago and the Antarctic Peninsula (Fig. 1a, b; Barker et al. 1991). The Bransfield Trough is a marginal basin situated at the rear of the inactive South Shetland Islands volcanic arc (Fretzdorff et al. 2004), formed as a consequence of the subduction of the former Phoenix Plate under the Antarctic Plate during Mesozoic–Cenozoic times (Dalziel 1984) and the interaction with the westward motion of the Scotia–Antarctic plate boundary

along the South Scotia Ridge (González-Casado et al. 2000). The Phoenix Ridge spreading ceased ~4 Myr ago (Lawver et al. 1996), although subduction continued along the South Shetland Trench (Maldonado et al. 1994). The Bransfield Trough extends toward the NE with the western part of the E–W trending South Scotia Ridge through a deep trough interpreted as a transtensional basin (Canals et al. 1992; Acosta et al. 1994; Galindo-Zaldívar et al. 1996, 2004). The East Scotia Sea is an active back-arc basin. Deception and Bridgeman islands are highs that divide the Bransfield Trough into western, central and eastern basins. The leftlateral plate boundary (along the South Scotia Ridge) forms the southern boundary of the Scotia Plate (Fig. 1c).

Several volcanic centers in the northern Antarctic Peninsula have the potential to disperse volcanic ash over large areas. The record of Quaternary volcanism from Bransfield Trough, the South Shetland Islands and surrounding seas, mostly in the form of tephra deposits, identifies Deception, Penguin and Bridgeman islands as the most active sources with lesser contributions from James Ross Island, seamounts and ridges, some of which may also be active (Kraus et al. 2013; Weaver et al. 1979; González-Ferrán 1985; Fisk 1990; Keller and Fisk 1992; Gràcia et al. 1996; Smellie et al. 2008).

The volcanic ridges and spurs in the Bransfield Trough are parallel to the NE–SW basin axis, which is divided by strike-slip faults (oriented mainly NW–SE) (Fig. 1c; Grad et al. 1992). An extensional fault system orientated NW– SE, together with a conjugate group of NE–SW normal oblique-slip faults, is present in the northern margin of the central Bransfield Basin (González-Casado et al. 1999). The recent tectonic evolution of the Bransfield Trough is controversial and explained by three different models: (1) Opening of the basin may be related to passive subduction of the former Phoenix Plate and rollback of the South Shetland Trench (e.g., Smellie et al. 1984; Maldonado et al. 1994; Lawver et al. 1995); (2) the sinistral movement between the Antarctic and Scotia plates may be causing an oblique extension along the Antarctic Peninsula continental margin. This extension generates the Bransfield Trough and defines the South Shetland tectonic block (Rey et al. 1995; Klepeis and Lawver 1996; Lawver et al. 1996; González- Casado et al. 2000); or (iii) both mechanisms cited before could occur simultaneously (Galindo-Zaldívar et al. 2004; Maestro et al. 2007).

Volcanism in Deception Island evolved during the Quaternary from pillow lavas to strombolian and phreatomagmatic subaerial eruptions. The volcanic deposits are divided into pre-caldera and post-caldera units (Smellie and López-Martínez 2000; Smellie 2001, 2002; Fig. 2). The pre-caldera units are named Port Foster Group, which includes from bottom to top Fumarole Bay (F1), Basaltic Shield (F2) and Outer Coast Tuff (F3) formations. They include subaqueous strombolian (likely fire-fountaining) deposits (F1), subaerial lavas (F2) and pyroclastic density current deposits (F3) that record the progressive evolution from submarine to subaerial volcanism (Smellie and López-Martínez 2000) and include mainly mafic rocks (Galé et al. 2014; and references therein). The Fumarole Bay Fm is interpreted as mostly subaqueous and originated from several coalesced centers (Hawkes 1961; Smellie 2002). The Basaltic Shield

Fm is basically composed of dry effusive and minor pyroclastic subaerial material. It is interpreted as a small shield volcano with at least two centers (Smellie 2002). The Outer Coast Tuff Fm is the result of a large eruption just prior to the caldera collapse and probably genetically related to the caldera collapse (Smellie 2002). This unit consists mainly of pyroclastic material, and it is widespread distributed through the island, draping unconformably on the Fumarole Bay and Basaltic Shield Fms. It is cut by a caldera fault, indicating that it represents products of the final eruption prior to (or possibly during) formation of the caldera (Smellie 2001, 2002). It was also suggested that the vent(s) of the Outer Coast Tuff Fm were below sea level (Smellie 2002). These deposits scarcely crop out since post-caldera materials cover them but they are well exposed in (largely inaccessible) cliffs of the outer coast and in some inner caldera wall sections. Martí et al. (2013) consider Outer Coast Tuff Fm as a syn-caldera collapse deposit, suggesting that the caldera subsidence occurs prior to its deposition. The post-caldera units consist of small-volume phreatomagmatic eruptions scattered across the island (hydrovolcanic tephra, lavas, tuff cone and maar deposits) and magmatic eruptions (strombolian scoria and lavas) of basaltic to dacitic composition (Smellie 2002; Galé et al. 2014 and references therein), mainly originated from multiple centers and from bottom to top include Baily Head and Pendulum Cove formations (Smellie and López-Martínez 2000; Smellie 2001). Almost time equivalent to the previous formations are Kendall Terrace Member (at least partly older than Baily Head Fm) and Stonethrow Ridge Fm (Mt Kirkwood Member), which is time equivalent to Pendulum Cove Fm.

Age of Deception Island

The relative ages of the individual volcanic units of Deception Island are comparatively well known; however, their absolute ages are not. Previous paleomagnetic data indicate that all rocks cropping out record normal magnetic polarity, what leads to infer an age younger than 780 ky (time of the last inversion of the magnetic poles; Valencio et al. 1979; Baraldo et al. 2003).

Attempts to date the volcanic events of Deception Island include radiometric dating of rocks from the island and tephras from ice, in addition to lacustrine and marine sediments around the Antarctic Peninsula. Radiometric K–Ar dating on whole rock suggests an age younger than 150 ky (±50 ky) for the subaerial volcanism of gray lava from Telefon Ridge (Keller et al. 1991), although it is considered too old and likely unreliable by Smellie (2001), because the sampled area corresponds to post-caldera eruptions the Stonethrow Ridge Fm, which includes historically documented eruptions from the XIX and XX centuries. Other information related to absolute dating comes from 14C of organic material associated with tephras from the Antarctic Peninsula area (ice, lakes and marine sediments). The geochemical compositions of the glass shards show that Deception Island is the major source of Quaternary tephra horizons in the northern Antarctic Peninsula region (Smellie 1990, 1999; Björck et al. 1991a; Hodgson et al. 1998; Pallàs et al. 2001; Lee et al. 2007). Moreton (1999) analyzed a megascopic ash layer recovered from six sediment cores from the Scotia and Weddell seas. This deposit represents the most extensive late Quaternary tephra known to be deposited in the northern Antarctic Peninsula region and Deception Island is

unambiguously identified as the source. The megascopic tephra layer has been 14C dated as 10,670 BP (Moreton 1999), and it is tentatively attributed to the eruption that immediately preceded and directly led to the caldera formation on Deception Island. The dating of the megascopic tephra layer is tentative as there are large discrepancies between the radiocarbon ages obtained from the sediments above and below the tephra layer in different cores and there are still large uncertainties regarding the magnitude of the marine reservoir effect at the time of the eruption (Moreton 2015 pers. comm.). Below the megascopic tephra, five other tephras can be correlated with varying extents between the central Scotia Sea cores. Deception Island has been identified as the source of all correlatable tephras. Three of these tephras have been radiocarbon-dated to 21,660 BP, 26,400 BP and 35,400 BP (the two oldest correlatable tephras have not been directly dated; Moreton 1999). Smellie (2001) considers that exposed rocks in Deception Island appear to be Late Pleistocene-Recent (probably <100 ka).

Studied materials and previous paleomagnetic data

The new paleomagnetic sites of the pre-caldera units (Smellie and López-Martínez 2000) are located in volcanic breccia and pillow lava of the Fumarole Bay Fm (F1, 4 sites) and in lavas of the Basaltic Shield Fm (F2, 1 site) (Tables 1, 2, 3; Figs. 2, 3). These outcrops are located in the no-collapsed area of the volcano, and the sampled lavas show low to moderate dips. The new paleomagnetic sites of the post-caldera units (Smellie and López-Martínez 2000) are located in lavas and, from younger to older, in the Kendall Terrace Member (scoria and lavas) (S1), in the lavas of the Collins Point cones (P2, which are partly equivalent in age to S2), and in the Stonethrow Ridge Fm, consisting of strombolian scoria and lavas (S2). The S1 unit drapes the caldera rim and has cascaded down the inner surface (Smellie 2002). It has been studied in 6 sites all around the island. The dikes were probably emplaced contemporaneously to the S1 unit, and in the sampled sites cut pre-caldera units [Fumarole Bay Fm and Outer Coast Tuff Fm, F1 and F3 units, respectively, of Smellie and López-Martínez (2000), Smellie (2002)] and post-caldera units [Baily Head Fm, P1 unit of Smellie and López-Martínez (2000), Smellie (2002)]. The P2 unit was sampled in three sites in Collins Point, to investigate possible local post-cooling deformations in the lavas as it was suggested by the outcrop appearance. The P2 unit is partly equivalent in age to S2 unit, but this last formation extended longer in time; however, for the discussion of the results, both units are combined into S2 unit. Later historical volcanic episodes are registered from 1829 to 1970 AD (from P3 to P8 units but considered S2 for this study) following descriptions of Smellie and López-Martínez (2000). Seventeen sites studied by Baraldo et al. (2003) were also taken into consideration (Table 4). These sites come from F2 (2 sites), F3 (6 sites), S2 (8 sites) units of Smellie and López-Martínez (2000), and one site from 1840 AD (considered together with S2 sites). Previous paleomagnetic studies performed in the Bransfield Trough, South Shetland Islands, Antarctic Peninsula and Patagonia pursued two different goals. On the one hand, there are the paleogeographical reconstructions that seek to unravel the tectonic evolution of the area since the Paleozoic (e.g., Poblete et al. 2011). And on the other hand, the paleomagnetic studies that focus in the more recent volcanic

rocks in order to study the evolution of the Earth's magnetic field and its secular variations (Baraldo et al. 2003). More specifically, previous paleomagnetic studies in Deception Island conclude that the low coercive magnetic minerals in the lavas averaged out the paleosecular variations, being the calculated mean direction no more than 2° far from the geocentric axial dipole direction model (Baraldo et al. 2003).

Methods and paleomagnetic analysis

The sampled sites were chosen looking for the most complete stratigraphic record of the Deception Island volcanism. Mostly, lavas and dikes have been studied, in addition to 4 sites from F1 unit (volcanic breccias—3 sites—and pillow lavas—1 site—). In the lavas, sampling was performed far from their external areas to avoid problems linked to a faster cooling when the lava still moves and/or possible interactions with underneath and subsequent volcanic episodes, considering that in certain cases the underlying magnetized bodies can affect the paleomagnetic records, for example, during periods of reduced field intensity as in reversals (Valet and Soler 1999). In two sites (5, 12), this has not been possible and we sampled the scoriaceous crust of the lava. The sampling was done in the field with a portable gasoline drill machine cooled with water. Drilled cores were oriented with an inclinometer and a compass. The 157 standard samples (2.5 cm in diameter and 2.1 cm in height), from 20 sites (Fig. 2), were thermally demagnetized at the paleomagnetic laboratory of University of Barcelona- CSIC using Schonsted and MMT80 furnaces. Furnaces were used to progressively heat the samples (from an initial room temperature to 580 °C) in 11–14 steps (every 50–20 °C) until complete demagnetization has occurred. The remanence was measured in a JR5 (AGICO Inc. Brno, Czech Republic). A stable component is calculated with good quality in 92 % of the samples. Stable directions are defined by visual inspection of the demagnetization diagrams with Remasoft 3.0 (Chadima and Hrouda 2006) and VPD (Ramón and Pueyo 2014). The stable component is computed at high temperature with more than 6 steps and maximum angular deviations (MADs) less than 5°. The method of calculation is by principal component analyses (PCA; Kirschvink 1980). The maximum unblocking temperatures range from 350 to 580 °C, which suggests titanium-rich magnetite and magnetite as carriers of the magnetization (Baraldo et al. 2003; Pueyo-Anchuela et al. 2014). Stereoplots were done with Cardozo and Allmendinger (2013) OSXSteronet software. Acquisition of isothermal remanent magnetization curves (IRM) were performed on selected samples with an Impulse Magnetizer IM10-30 (ASC Scientific) applying a maximum field of 1 T to obtain more information about the ferromagnetic carriers.

Paleomagnetic results

The paleomagnetic characteristic component has been calculated successfully in 88 % of the analyzed samples. The ferromagnetic carrier is of very low coercivity as seen in the acquisition curves of the isothermal remanent magnetization (Fig. 4) and by previous results (Baraldo et al. 2003). The average of the natural remanent magnetization (NRM) at every site ranges from 0.05 to 20 A/m, except for site 12, which is almost 40 A/m. The NRM average

has a value of 9.1 with a standard deviation of 4.4 A/m (without taking into account site 12; Fig. 5).

Demagnetization diagrams of selected samples are shown in Fig. 6, and the average component for every site is in Table 3. The mean inclinations vary from −56° (site 5) to −85° (site 9), and declinations from 319° (site 1) to 16° (site 5). The expected inclination for Deception Island at latitude 63°S is: INC = 75.7° following the dipole formula for the Earth magnetic field (tan λ = 0.5 * tan INC, where λ is the latitude). Paleomagnetic data at high latitudes have the drawback of the error associated with high inclinations since the paleomagnetic inclination is related to latitude. The error in declination for a site (averaging 8 or 7 samples) is calculated dividing the α95 by the cosine of the magnetic inclination (εDEC ~ α95/ cos INC). Therefore, the higher the magnetic inclination, the higher the uncertainty of the declination. The fisherian parameter α95 represented by the semi-apical angle of a cone that revolves around the average and where the 95 % of the data (with normal distribution) is contained, is also a measure of the concentration of the average for a site; therefore, the higher the α95, the higher the error in declination. Errors in the α95 for Deception Island are indicated in Table 3. In average, they are very low, α95 < 5°, except for the oldest rocks (F1 unit), which are volcanic breccias (and one site in pillow lavas). Consequently, the error in paleomagnetic declination for the latitude of Deception Island will be (in average) equal to 5° divided by cosine of 75.7° (cosine of the expected inclination), which is ~19°.

Discussion

The paleomagnetic data, apart from detecting rotations (or lack of them) in multiple tectonic scenarios (e.g., Van der Voo 1993; Sussman and Weil 2004), can have another application in volcanic contexts, i.e., use the variation of the geomagnetic field recorded in volcanic rocks as a correlating tool of eruptions, so long as the volcanic units have not undergone tilting through post-depositional volcanic or unrelated tectonic processes (Doell and Cox 1963). In addition, paleomagnetic data from well-dated volcanic (e.g., Carlut et al. 2000; Tauxe et al. 2004) and from archaeomagnetic materials (e.g., Gómez-Paccard et al. 2006) are used to construct geomagnetic models (e.g., Pavón-Carrasco et al. 2014) that allow changes of the Earth's magnetic field at the surface to be calculated. Therefore, any undated paleomagnetic data can be compared at any location with the geomagnetic model for dating purposes (e.g., Gómez-Paccard and Beamud 2008; Speranza et al. 2008; Kissel et al. 2015).

The time of the acquisition of the thermoremanent magnetization (TRM) (paleomagnetic vector) in a volcanic deposit occurs when the material (lavas, ignimbrites, pyroclasts, tephras) cools down below TRM acquisition temperature, which is the Curie temperature. Just below the Curie temperature, the ferromagnetic *s.l.* minerals (Fe–Ti-oxides) change from paramagnetic to ferromagnetic *s.l.*, precisely at that time they record the Earth magnetic field. The Curie temperature depends more specifically on the chemical composition of the ferromagnetic mineral; e.g., for pure magnetite, it is 580 °C and decreases as titanium enters in the structure (Dunlop and Özdemir 1997). Therefore, the acquisition time of the remanent magnetization is close to the

eruption time, since eruption temperatures range from 1600 °C (more basic lavas) to 900 °C (Griffiths 2000 and references therein). As an example, in Hawaii a lava flow with an eruption temperature of about 1150 °C in 52 min descends to ~400 °C (Flynn and Mouginois-Mark 1992).

The cooling rate for dikes is higher, but also depends on diffusivity, depth of emplacement, composition and especially dike thickness. Depending on the last condition, time of cooling obtained from a thermal modeling in aplite–pegmatite dikes can vary from ~9 years to 5 days for a 25-mto 1-m-thick dike, respectively (Webber et al. 1999). For ignimbrites and other volcanic breccias, the acquisition of a stable characteristic remanent magnetization also depends on the time of cooling down below the temperature for the TRM acquisition. Therefore, paleomagnetic data are used to calculate temperatures of emplacement (Porreca et al. 2006). Recently, it has been suggested that densely welded pyroclastic deposits record accurately the ambient geomagnetic field direction at the time of emplacement; on the contrary, non-welded pyroclastic deposits show large confidence limits or deviations from their expected directions due to modification of remanence direction introduced from random rotations of remanence-carrying material during syn- or post-depositional stages (Uno et al. 2014).

Secular variations, age and cooling rate differences among sites

When magnetic vectors of the same unit (and therefore of the same age) group well in the in situ position, the displacements of the volcanic deposits after cooling down below TRM acquisition temperature are minimal. On the contrary, when a local post-emplacement rotation occurs, the paleomagnetic vectors will be more scattered in the in situ position than in the previous case. Conversely, due to geomagnetic secular variation, when two distinct volcanic deposits show statistically separate and well-characterized TRMs, and deformation has not taken place, that indicates a significant time interval (>100 years) elapsed between deposits, confirming the existence of two different volcanic events (Paquereau-Lebti et al. 2008). Baraldo et al. (2003) have already determined that PSV are averaged out in Deception Island. In Deception Island, we compare only sites within the same volcanic unit in a broad sense, with respect to time. Since there is a lack of a good age constraint in rocks cropping out at Deception Island, a total of five main groups are considered, following divisions from Smellie and López- Martínez (2000): (1) three pre-caldera groups or units, F1, F2 and F3, and (2) two post-caldera groups or units, S1 (including dikes) and S2. For the pre-caldera studied materials, F1 was subaqueously originated from different vents, some of which were co-eruptive (Smellie 2001). The F1 unit is divided into three members that are, from older to younger, F1a (hyaloclastite breccia and lava), F1b (palagonitized scoria member: lapillistone and coarse grain lapilli tuff) and F1c (well-stratified yellow lapillistone and lapilli tuff). They can be recognized in the field as three distinct deposits that formed progressively within single vents as a result of progressive shoaling and variations in the proportion of external water available (Smellie 2001, 2002). The lavas sampled in the F2 unit (a subaerial lava shield) seems originated in one single vent, but that is not so clear for F3, where the volume of erupted material is calculated as 30–90 km3, quite large

for the island and with significant involvement of water (Baraldo and Rinaldi 2000; Smellie 2001, 2002; Martí et al. 2013). Therefore, any large differences in magnetic declination or inclination among sites of these units might be related to tilting. The post-caldera collapse units encompass a higher variability in eruption timing (especially S2 group) and also in space; they originated from multiple centers (Smellie and López-Martínez 2000); consequently, any differences in the magnetic signal (declination and inclination) among sites can be attributable not only to possible tilting but also to secular variations due to age difference. On top of that, possible discrepancies among sites or within sites (higher scattering of paleomagnetic data within a site) can be due to very fast cooling before final deposition, then the TRM will be scattered or TRM can show at least 2 components, and the characteristic component can be scattered above certain temperature (Porreca et al. 2006), this will be more probable to occur in volcanic breccia or scoriaceous lavas than in lavas, since cooling rates are expected to be faster in the former.

Paleomagnetic data are "untilted"

The five volcanic units are represented in Fig. 7 and Table 5. The magnetic inclination in Deception Island is large enough to likely mask subtle and local tilting among volcanic units [as seen in Gil-Imaz et al. (2010) and Pueyo- Anchuela et al. (2014)]. Large tilting variations affecting declination or inclination values have been detected in some site mean values in Baraldo et al. (2003). Rotation errors around a vertical axis will be larger in places with high magnetic inclination (as in Deception Island) because the error in paleomagnetic declination values for an average site depends on the cosine of the inclination. However, average values per unit from the new sites show good clustering: α95 less than 6 (except for F1 sites) and *k* (precisión parameter) higher than 198 (except for S2 and F1). α95 is the angle indicating that the unknown true mean direction lies within α95 of the calculated mean, and *k* value is higher and higher as the distribution is more and more concentrated at a point (Butler 1992). Therefore, paleomagnetic averaged values for F2, F3 and S1 suggest that sites among those units are not largely tilted. The large scattering of F1 sites can be explained considering that the lithology is indurated volcanic breccia (all sites but one, which is taken in pillow lavas). The aerial volcanic breccia cools down faster than lava flows and might begin to acquire the TRM before the deposition of the unit ceases (Porreca et al. 2006). Our interpretation for F1 unit differs from the aerial deposits, since aerial welded tuff deposits provide clustered paleomagnetic data (Uno et al. 2014). It is difficult to detect any possible tilting with F1 unit, but it is considered unlikely since F2 and F3 (also pre-caldera collapse units) show good clustering; then no large tilting in the pre-caldera collapse units is occurring. Baraldo et al. (2003) found two sites within F2 unit with anomalous inclination values, suggesting some local tilting.

The possibility of recording different secular variations among sites with the F1 unit could be also another reason for the scattering observed among the 4 sites. However, the samples are from a single upwardly evolving eruptive structure (i.e., different stages from the same eruptive episode), and then the scattering is most probably related to the fast cooling in contact with water during ejection (Smellie 2001, 2002). The F3 unit is also a subaqueous deposit

(as F1 unit), mainly composed of indurated lapilli and breccias. The better clustering of this F3 unit with respect to F1 unit may be due to deposition of the unit while still hot (above Curie temperature). This would indicate that the pyroclastic density currents of F3 unit were very dense flows, and they were formed during water-rich phreatomagmatic eruptions associated with dense low-elevation eruption columns (Martí and Baraldo 1990) that prevented the rapid ingress of cooling seawater and thus remained at relatively high temperatures until deposition, when they then cooled relatively rapidly. This would result in consistent clustering (Smellie 2015 pers. comm.).

The scattering for S2 unit must be due to paleosecular variations among sites, i.e., eruptions took place at different vents at different times. Many different eruptions from different centers are grouped together in this unit. Again, we discard that large tilting occurs in this unit, since previous units (S1) are not scattered and, therefore, not affected by large tilting among sites.

Probable ages after comparing with geomagnetic model and tephra layers

When paleomagnetic data cannot detect possible tilting among sites of the same unit, combination of paleomagnetic declination and inclination with geomagnetic models will provide probable ages for each unit. Geomagnetic models predict the behavior of the Earth magnetic field using as anchor points well-dated and reliable paleomagnetic data (the characteristic component has a small error). The limitation is that they only extend as far as the last 14 ky, from 12,000 BC to 1900 AD (Pavón- Carrasco et al. 2014). This recently developed geomagnetic model uses only paleomagnetic data from archaeomagnetic and lava data, avoiding sediments. In an attempt at providing dates for the five different volcanic units, we have compared the new paleomagnetic data (combined with 17 sites from Baraldo et al. 2003) with the declination and inclination obtained from the geomagnetic model for the position of Deception Island (http://pc213fis.fis.ucm.es/sha.dif.14k/index.html; Pavón-Carrasco et al. 2014; Fig. 8). We then consider only the average data (without errors) from the geomagnetic model and the paleomagnetic data from Deception Island. The age estímate is established when declinations and inclinations (horizontal colored lines crossing the average geomagnetic model values) converge at one time (vertical dashed line; see Fig. 8). The age error deduced for the volcanic units in Deception Island varies from 150 year (S1 unit) to ~1000 year (S2 unit). From that, it can be observed that there is only one posible age for S1 unit, which occurs at ~2000 year BC; therefore, the timing of the other units will make sense when considering this anchor point. S2 unit shows two possible ages with this approach (both younger than 1900 year BC) that cover a time interval between around 1700 and 1250 year BC. F3 unit has two probable options in ~8300 year BC and ~2400 year BC. The youngest estimated age for F3 unit is less probable because the inclination and declination do not exactly overlap at the same time. For F2 and F1 units, there is no overlapping of declination and inclination average values at the same time. Therefore, we consider them to be older than 12,000 year BC. Notwithstanding the lack of clustering for the average new paleomagnetic value of F1 unit, we still considered the average as in the other units, and only younger ages than

2000 year BC would be probabilistically possible (not marked with vertical dashed lines in Fig. 8). Therefore, we consider F1 to be older than 12,000 year BC. Tephra correlation studies with an origin in the Deception Island eruptions are compiled in Smellie (1999) and Moreton (1999). From those dates, it is worth mentioning that the megascopic tephra layer dated with 14C at 10,670 BP (or 8720 BC, Fig. 8) in Moreton (1999) is considered as related to the eruption that immediately preceded and directly led to the caldera formation on Deception Island. That dating occurs before the age of the F3 paleomagnetic deduced dating. Therefore, F3 unit could be considered related to that eruptive event. Older tephra layers from Moreton (1999) are correlated with absolute ages and occur before 12,000 year BC. However, younger tephra occurrences in the Antarctic Peninsula are more abundant than the deduced paleomagnetic datings. Nevertheless, the eruptive period between 1150 and 1950 year BC probability originated from explosive phreatomagmatic eruptions (Matthies et al. 1990, compiled in Smellie 1999) overlaps with the paleomagnetic deduced dates for S1 and S2 units. However, these units correspond to strombolian and weakly explosive eruptions, which are unlikely sources for any of the tephras deposited in the region, so this apparent correlation in timing could be unreal.

Reliability of the geomagnetic model and dating method

There are two data sets to assess the reliability of the geomagnetic model and dating method: (1) the historic eruption occurring at 1842 AD (paleomagnetic data from Baraldo et al. 2003) which lies near the geomagnetic model (see black squares and error bars in Fig. 8), although the perfect overlapping occurs at 1900 AD, then an error of 58 year can be account for; and (2) the average of the historic eruptions from S2 unit (data in this paper). The average data for the S2 unit incorporate different eruptions from different time and areas. Nonetheless, considering that most of the eruptions comprised in S2 are historic (XIX and XX centuries), they should locate on the right side of Fig. 8. However, the youngest probable age for S2 is ~1250 year BC, and as a result about at least 3000 year error can be considered for this unit. The methodology used in the paper to give an absolute probable age per volcanic unit is definitely biased by the averaged itself; as a consequence, the second error assessment can account for both the dating method and the geomagnetic model. Nonetheless, an estimation of when the volcanic units occur, in average, is determined with paleomagnetic data.

The temporal closeness of F3 unit (~8300 year BC) with the tephra related to the eruption that immediately preceded the caldera at ~8720 year BC (Moreton 1999) suggests that the averaged paleomagnetic data, despite all weaknesses, provide reasonable results when secular variation is averaged.

Conclusions

The new paleomagnetic results of 20 sites of pre- and postcaldera units and dikes indicate a good record of the Earth's paleomagnetic field. In addition, prior results suggest that the secular variations of such magnetic field are averaged out in Deception Island.

The paleomagnetic results suggest that none of the selected volcanic units experienced large tilting since their emplacement. Despite the uncertainties in the use of averaged paleomagnetic data for volcanic units, the new paleomagnetic data allow probable ages of volcanic units on Deception Island to be determined by comparing the paleomagnetic data with the geomagnetic model of Pavón-Carrasco et al. (2014). Our results in combination with tephra occurrences suggest that the pre-caldera collapse units F1 and F2 erupted before 12,000 year BP, the caldera collapse took place at about 8300 year BC, whereas S1 unit erupted at ~2000 year BC and S2 unit is younger than 1900 year BC.

Acknowledgments The authors express their gratitude to the personnel of the Gabriel de Castilla Antarctic station, for the logistic support. This work was supported by the Projects CTM2011- 13902E, CTM2011-26372 and CTM214-57119-R of the Spanish National R&D Plan. The authors are also very grateful to the reviewers J.L. Smellie and S. Moreton for their valuable and constructive

References

Acosta J, Canals M, Alonso B, ORCA Group (1994) Bathymetry of the Hesperides Deep, Scotia Sea, South Scotia Ridge, Antarctica. Map scale 1:200,000. GRGM (eds), University of Barcelona, Barcelona

Baker PE, McReath I, Harvey MR, Roobol MJ, Davies TG (1975) The geology of the South Shetland Islands: V. The volcanic evolution of deception Island. Br Antarct Surv Sci Reps 78:1–81

Baraldo A, Rinaldi CA (2000) Stratigraphy and structure of Deception Island, South Shetland Island, Antarctica. J S Am Earth Sci 13:785–796

Baraldo A, Rapalini AE, Böhnel H, Mena M (2003) Paleomagnetic study of Deception Island, South Shetland Islands, Antarctica. Geophys J Int 153:333–343

Barker DHN, Austin JA (1994) Crustal diapirism in Bransfield Strait, West Antarctica: evidence for distributed extension in marginalbasin formation. Geology 22:657–660

Barker PF, Dalziel IWD, Storey BC (1991) Tectonic development of the Scotia Arc Region. In: Tingey RJ (ed) Antarctic geology. Oxford University Press, Oxford, pp 215–248

Birkenmajer K (1992) Volcanic succession at Deception Island, West Antarctica: a revised lithostratigraphic standard. Stud Geol Pol 101:27–82

Björck S, Hákansson H, Zale R, Karlén W, Liedberg-Jönsson B (1991a) A late Holocene lake sediment sequence from Livingston Island, South Shetland Islands, with palaeoclimatic implications. Ant Sci 3:61–72

Björck S, Sandgren P, Zale R (1991b) Late Holocene tephrochronology of the northern Antarctic Peninsula. Quat Res 36:322–328

Butler RF (1992) Paleomagnetism. Magnetic domains to geologic terranes. Blackwell Sc Pub, 319 pp

Canals M, Acosta J, Gràcia E, Escartín J, Grupo ORCA (1992) Caracterización geológica de la región de enlace entre la Cuenca de Bransfield y la Dorsal Sur de Scotia (Antártida). Acta Geol Hisp 27:89–110

Cardozo N, Allmendinger RW (2013) Spherical projections with OSXStereonet. Comput Geosci 51:193–205. doi:10.1016/j.cageo.2012.07.021

Carlut J, Quidelleur X, Courtillot V, Boudon G (2000) Paleomagnetic directions and K/Ar dating of 0 to 1 Ma lava flows from La Guadeloupe Island (French West Indies): implications for time-averaged field models. J Geophys Res 105(B1):835–849. doi:10.1029/1999JB900238

Chadima M, Hrouda F (2006) Remasoft 3.0 a user-friendly paleomagnetic data browser and analyzer. Travaux Géophysiques XXVII: 20–21

Dalziel IWD (1984) Tectonic evolution of a fore-arc terrane, Southern Scotia Ridge, Antarctica. Geol Soc of America Sp Paper 200, 32p

Doell RR, Cox A (1963) The accuracy of the paleomagnetic method as evaluated from historic Hawaiian lave flows. Geophys Res Lett 68:1997–2009. doi:10.1029/JZ068i007p01997

Dunlop DJ, Özdemir Ö (1997) Rock magnetism: fundamentals and frontiers. Cambridge University Press, Cambrige, 572 p

Fisk MR (1990) Volcanism in the Bransfield Strait, Antarctica. J S Am Earth Sci 3:91–101

Flynn LP, Mouginois-Mark PJ (1992) Cooling rate of an active Hawaiian lava flow from nighttime spectroradiometer measurements. Geophys Res Lett 17:1783–1786

Fretzdorff S, Worthington TJ, Haase KM, Hékinian R, Franz L, Keller RA, Stoffers P (2004) Magmatism in the Bransfield Basin: rifting of the South Shetland Arc? J Geophys Res 109:B12208. doi:10.1029/2004JB003046

Funaki M, Sakanaka S, Higashimno S-I (2012) The first successful aeromagnetic survey by an autonomous unmanned aerial vehicle, AntPlane 6-3, in Antarctica. 13th Castle Meeting, Zvolen Slovakia. Abstracts

Galé C, Ubide T, Lago M, Gil-Imaz A, Gil-Peña I, Galindo-Zaldívar J, Rey J, Maestro A, López-Martínez J (2014) Vulcanismo cuaternario de la Isla Decepción (Antártida): una signatura relacionada con la subducción de la Fosa

de las Shetland del Sur en el dominio de tras-arco de la Cuenca de Bransfield. Bol Geol y Min 125(1):31–52

Galindo-Zaldívar J, Jabaloy A, Maldonado A, De Galdeano CS (1996) Continentalfragmentation along the South Scotia Ridge transcurrent plate boundary (NE Antarctic Peninsula). Tectonophysics 258(1):275–301

Galindo-Zaldívar J, Gamboa L, Maldonado A, Nakao S, Bochu Y (2004) Tectonic development of the Bransfield Basin and its prolongation to the South Scotia Ridge, northern Antarctic Peninsula. Mar Geol 206(1):267–282

Gil-Imaz A, Gil-Peña I, Galindo-Zaldívar J, Rey-Salgado J, Maestro- González A, Pueyo-Anchuela Ó, Soto-Marín R, Oliva-Urcia B, López-Martínez J (2010) Magnetic fabric significance of quaternary volcanic rocks of Deception Island (South Shetland Islands, Antarctica). Geogaceta 49:103–106

Gómez-Paccard M, Beamud E (2008) Recent achievements in archaeomagnetic dating in the Iberian Peninsula: application to four Spanish structures. J Archaeol Sci 35:1389–1398. doi:10.1016/j.jas.2007.10.005

Gómez-Paccard M, Catanzariti G, Ruiz-Martínez VC, McIntosh G, Núñez JI, Osete ML, Chauvin A, Lanos PH, Tarling DH, Bernal- Cassola D, Thiriot J, Archaeological Working Group (2006) A catalogue of Spanish archaeomagnetic data. Geophys J Int 166:1135–1143

González-Casado JM, López-Martínez J, Durán JJ (1999) Active tectonics and morphostructure at the northern margin of the central Bransfield Basin, Hurd Peninsula, Livingston Island (South Shetland Islands). Ant Sc 11:323–331

González-Casado JM, Giner J, López-Martínez J (2000) Bransfield Basin, Antarctic Peninsula: not a normal backarc basin. Geology 28(11):1043–1046

González-Ferrán O (1985) Volcanic and tectonic evolution of the northern Antarctica Peninsula—Late Cenozoic to Recent. Tectonophysics 114:389–409

Gràcia E, Canals M, Farrán M, Prieto MJ, Sorribas J, GEBRA Team (1996) Morphostructure and evolution of the Central and Eastern Bransfield Basins (NW Antarctic Peninsula). Mar Geophys Res 18:429–448

Grad M, Guterch A, Sroda P (1992) Upper crustal structure of Deception Island Area, Bransfield Strait, West Antarctica. Ant Sci 4:469–476

Griffiths RW (2000) The dynamics of lava flows. Ann Rev Fluid Mech 32:477–518

Hall B, Henderson G (2001) Use of uranium–thorium dating to determine past 14C reservoir effects in lakes—examples from Antarctica. Earth Plan Sci Lett 193:565–577

Hawkes DD (1961) The geology of the South Shetland Islands: II. The geology and petrology of Deception Island. Falkland Islands Dependencies Survey Scientific Reports 27, 43

Hjort C, Ingólfsson Ó, Möller P, Lirio JM (1997) Holocene glacial history and sealevel changes on James Ross Island, Antarctic Peninsula. J Quat Sci 12:259–273

Hodgson DA, Dyson CL, Jones VJ, Smellie JL (1998) Tephra analysis of sediments from Midge Lake (South Shetland Islands) and Sombre Lake (South Orkney Islands), Antarctica. Ant Sci 10(1):13–20

Ingólfsson Ó, Hjort C, Björck S, Smith RIL (1992) Late Pleistocene and Holocene glacial history of James Ross Island, Antarctic Peninsula. Boreas 21:209–222

Keller R, Fisk MR (1992) Quaternary marginal basin volcanism in the Bransfield Strait as a modern analogue of the Southern Chilean Ophiolites. In: Parson LM, Murton BJ, Browning P (eds) Ophiolites and their modern oceanic analogues. Geol Soc London Spec Publ, vol 60, pp 155–169

Keller RA, Fisk MR, Birkenmajer K (1991) Isotopic and trace element constraints on mixing and melting models of marginal basin volcanism, Bransfield Strait, Antarctica. Earth Plan Sci Lett 111:287–303

Kirschvink JL (1980) The least-squares line and plane and the analysis of paleomagnetic data. Geophys J Int 62:669–718

Kissel C, Rodríguez-González A, Laj C, Pérez-Torrado F, Carracedo JC, Wandress C, Guillou H (2015) Paleosecular variation of the earth magnetic field at the Canary Islands over the last 15 ka. Earth Plan Lett 412:52–60

Klepeis KA, Lawver LA (1996) Tectonics of the Antarctic–Scotia plate boundary near Elephant and Clarence Islands, West Antarctica. J Geophys Res 101(B9):20211–20231

Kraus S, Kurbatov A, Yates M (2013) Geochemical signatures of tephras from Quaternary Antarctic Peninsula volcanoes. Andean Geology 40(1):1–40. doi:10.5027/andgeoV40n1-a01

Lawver LA, Keller RA, Fisk MR, Strelin J (1995) Bransfield Strait, Antarctic Peninsula active extension behind a dead arc. In: Taylor B (ed) Backarc Basins: tectonics and magmatism. Plenum Pub Corp, New York, pp 315–342

Lawver LA, Sloan BJ, Barker DHN, Ghidella M, Von Herzen RP, Keller RA, Klinkhammer GP, Chin CS (1996) Distributed, active extension in Bransfield Basin, Antarctic Peninsula: evidence from multibeam bathymetry. GSA Today 6:1–6

Lee YI, Li HS, Yoon HI, Tatur A (2007) Characteristics of tephra in Holocene lake sediments on King George Island, West Antarctica: implications for deglaciation and paleoenvironment. Quat Sci Rev 26:3167–3178

López-Martínez J, Serrano E, Rey J, Smellie JL (2000) Geomorphological map of Deception Island. BAS GEOMAP Series, Sheet 6-B, 1:25,000. British Antarctic Survey, Cambridge

Maestro A, Somoza L, Rey J, Martínez-Frías J, López-Martínez J (2007) Active tectonics, fault pattern and stress field of Deception Island: a response to oblique convergence between the Pacific and Antarctic plates. J S Am Earth Sci 23:256–268

Maldonado A, Larter RD, Aldaya F (1994) Forearc tectonic evolution of the South Shetland Margin, Antarctic Peninsula. Tectonics 13:1345–1370

Martí J, Baraldo A (1990) Pre-caldera pyroclastic deposits of Deception Island (South Shetland Islands). Earth Sci Glaciol 2:345– 352. doi:10.1017/S0954102090000475

Martí J, Geyer A, Aguirre-Díaz G (2013) Origin and evolution of the Deception Island caldera (South Shetland Islands, Antarctica). Bull Volc 75(6):732

Matthies D, Mäusbacher R, Storzer D (1990) Deception Island tephra: a stratigraphical marker for limnic and marine sediments in Bransfield Strait area, Antarctica. Zbl Geol Paläont 1:153–165

Moreton SG (1999) Quaternary tephrochronology of the Scotia Sea and Bellingshausen Sea, Antarctica. PhD Thesis, Cheltenham and Gloucester College of Higher Education, UK, 164 p. http://store.pangaea.de/Publications/MoretonSG

Ortiz R, Vila J, García A (1992) Geophysical features of Deception Island. In: Yoshida Y, Kaminuma K, Shiraishi K (eds) Recent progress in Antarctic Earth Science. Terrapub, Tokyo, pp 443–448

Pallàs R, Smellie JL, Casas JM, Calvet J (2001) Using tephrochronology to date temperate ice: correlation between ice tephras on Livingston Island and eruptive units on Deception Island volcano (South Shetland Islands, Antarctica). Holocene 11(2):149–160

Paquereau-Lebti P, Fornari M, Roperch P, Thouret JC, Macedo O (2008) Paleomagnetism, magnetic fabric, and 40Ar/39Ar dating of Pliocene and quaternary ignimbrites in the Arequipa area, southern Peru. Bull Volcanol 70:977–997. doi:10.1007/s00445-007-0181

Pavón-Carrasco FJ, Osete ML, Torta JM, De Santis A (2014) A geomagneticfield model for the Holocene based on archaeomagnetic and lava flow data. Earth Planet Sci Lett 388:98–109

Poblete F, Arriagada C, Roperch P, Astudillo N, Hervé F, Kraus S, Le Roux JP (2011) Paleomagnetism and tectonics of the South Shetland Islands and the northern Antarctic Peninsula. Earth Planet Sci Lett 302:299–313

Porreca M, Giordano G, Mattei M, Musacchio P (2006) Evidence of two Holocene phreatomagmatic eruptions at Stromboli volcano (Aeolian Islands) from paleomagnetic data. Geophys Res Lett33:L21316. doi:10.1029/2006GL027575

Pueyo-Anchuela O, Gil-Imaz A, Gil-Peña I, Maestro A, Galindo- Zaldívar J, López-Martínez J, Rey J, Soto R, Oliva-Urcia B (2014) Application of AMS for reconstruction of the geological evolution of recent volcanic systems: case of Deception Island (South Shetland Islands, Antarctica). Tectonophysics 626:69–85.doi:10.1016/j.tecto.2014.03.032

Ramón MJ, Pueyo EL (2014) Virtual Paleomagnetic Directions. http://www.igme.es/internet/zaragoza/aplicaInfor.htm. Based on: Ramón and Pueyo, 2012. Automatic calculation of demagnetization intervals; a new approach based on the virtual directions and comparison with linearity spectrum analysis. Geotemas 13:1180–1183

Rey J, Somoza L, Martínez-Frías J (1995) Tectonic, volcanic and hydrothermal event sequence on Deception Island (Antarctica).Geo-Mar Lett 15:1–8

Rey J, Somoza L, Martínez-Frías J, Benito R, Martín-Alfageme S (1997) Deception Island (Antarctica): a new target for exploration of Fe–Mn mineralization? In: Nicholson K, Hein JR, Bühn B, Dasgupta S (eds), Manganese mineralization: geochemistry and mineralogy of terrestrial and marine deposits. Geol SocLondon Sp Publ 119, pp 239–251

Smellie JL (1990) Graham Land and South Shetland Islands. In: Le Masurier WE, Thomson JW (eds) Volcanoes of the Antarctic plate and southern oceans. Ant Res Series 48, pp 302–359

Smellie JL (1999) The upper Cenozoic tephra record in the south polar region: a review. Glob Planet Chang 21:51–70

Smellie JL (2001) Lithostratigraphy and volcanic evolution of Deception Island, South Shetland Islands. Ant Sci 13(2):188–209

Smellie JL (2002) Chronology of eruptions of Deception Island. In: López-Martínez J, Smellie JL, Thomson JW, Thomson MRA (eds) Geology and geomorphology of Deception Island, BAS GEOMAP Series, Sheets 6-A and 6-B. British Antarctic Survey, Cambridge, 70 p

Smellie JL, López-Martínez J (2000) Geological Map of Deception Island. BAS GEOMAP Series, Sheet 6-A, 1:25,000. British Antarctic Survey, Cambridge

Smellie JL, López-Martínez J (2002) Introduction. In: López-Martínez J, Smellie JL, Thomson JW, Thomson MRA (eds) Geology and geomorphology of

Deception Island, BAS GEOMAP Series, Sheets 6-A and 6-B. British Antarctic Survey, Cambridge, pp 1–6

Smellie JL, Pankhurst RJ, Thomson MRA, Davies RES (1984) The geology of the South Shetland Islands: VI. Stratigraphy, geochemistry and evolution. Brit Ant Surv Sci Rep 85

Smellie JL, Johnson JS, Mcintosh WC, Esser R, Gudmundsson MT, Hambrey MJ, Van Wyk De Vries B (2008) Six million years of glacial history recorded in the James Ross Island Volcanic Group, Antarctic Peninsula. Palaeogeogr Palaeoclimatol Palaeoecol 260:122–148

Speranza F, Pompilio MD'Ajello, Caracciolo F, Sagnotti L (2008) Holocene eruptive history of the Stromboli volcano: constraints from paleomagnetic dating. J Geophys Res 113:B09101. doi:10.1029/2007JB005139

Sussman A, Weil AB (2004) Classifying curved orogens based on timing relationships between structural development and verticalaxis rotations. In: Orogenic curvature: integrating paleomagnetic and structural analyses. Geol Soc Am Sp Paper 383, pp 1–12

Takahashi HA, Wada H, Nakamura T, Miura H (1999) 14C anomaly of freshwater algae in Antarctic coastal ponds and lakes. Polar Geosci 12:248–257

Tauxe L, Gans P, Mankinen EA (2004) Paleomagnetism and 40Ar/39Ar ages from volcanics extruded during the Matuyama and Brunhes Chrons near McMurdo Sound, Antarctica. Geochem Geophys Geosyst. doi:10.1029/2003GC000656

Uno K, Furukawa K, Ando H, Shinmura T, Miyoshi M (2014) Instantaneous record of the geomagnetic field direction of various facies from pyroclastic flow deposits: tests for consistency in paleomagnetic directions. Phys Earth Planet Int 235:96–106

Valencio DA, Mendía JE, Vilas JF (1979) Paleomagnetism and K–Ar age of Mesozoic and Cenozoic igneous rocks from Antarctica. Earth Planet Sci Lett 45:61–68

Valet JP, Soler V (1999) Magnetic anomalies of lava fields in the Canary Islands: possible consequences for paleomagnetic records. Phys Earth Planet Int 115:109–118

Van der Voo R (1993) Paleomagnetism of the Atlantic, Tethys and Iapetus oceans. Cambridge University Press, London, 411 p

Weaver SD, Saunders AD, Pankhurst RJ, Tarney J (1979) A geochemical study of magmatism associated with the initial stages of back-arc spreading: the

quaternary volcanics of Bransfield Strait from South Shetland Islands. Contr Miner Pet 68:151–169

Webber KL, Simmons WB, Falster AU, Foord EE (1999) Cooling rates and crystallization of shallow level pegmatite-aplite dikes, San Diego County, California. Am Miner 84:708–717

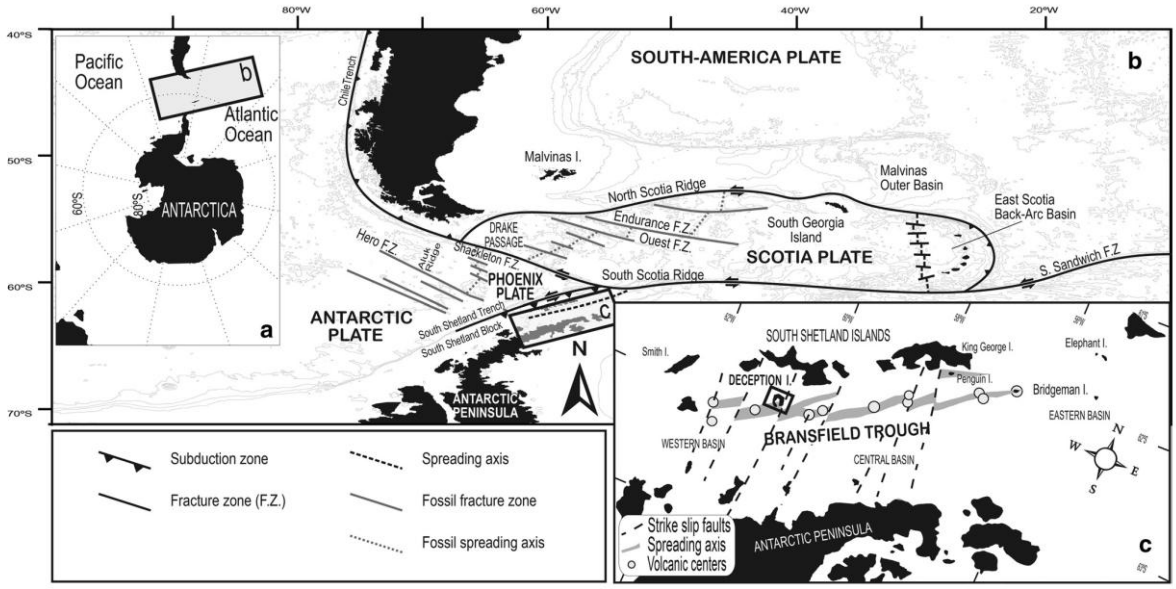

945 **Fig. 1** Tectonic setting. **a**, **b** Location and regional tectonic framework of the
946 Scotia Arc, northern Antarctic Peninsula region and Deception Island. The
947 Bransfield Trough area is marked by a *box*. **C** Tectonic and geographical
948 location of Deception Island north of the spreading axis of the Bransfield Trough
949 [modified from Grad et al. (1992), Barker and Austin (1994), Rey et al. (1997)]

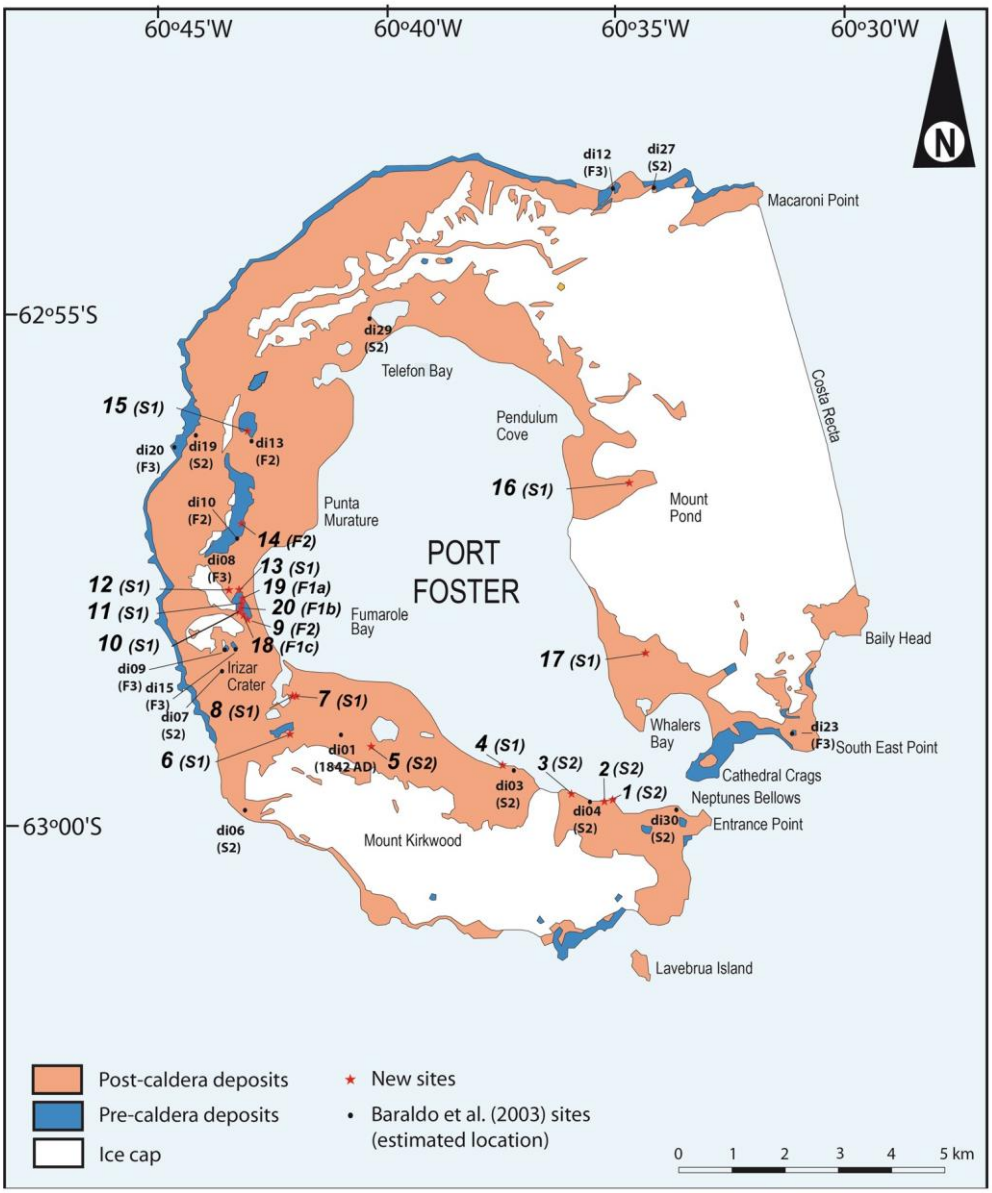

950 **Fig. 2** Location of the studied paleomagnetic sites in Deception Island.
951 Simplified geological map in the background taken from Smellie and López-
952 Martínez (2000)

Fig. 3 Photographs showing features of some of the sampling sites **a** basaltic dike at site 8; **b** basaltic dike that cuts the Outer Coast Tuff Formation at 6; **c** basaltic lava of S2 unit at site 5; **d** basaltic lava discordant on Baily Head Formation at site 17; **e**, **f** the sites 2 and 1, respectively, are located in the western part of the basaltic lava of P2 unit in Collins Point; **g** Basaltic pillow lava of F1c unit in Fumarole Bay Formation at site 9; and **h** Basaltic lava of Basaltic Shield Formation at site 14. The names of the lithostratigraphic units are in all cases according to Smellie and López-Martínez (2000, 2002)

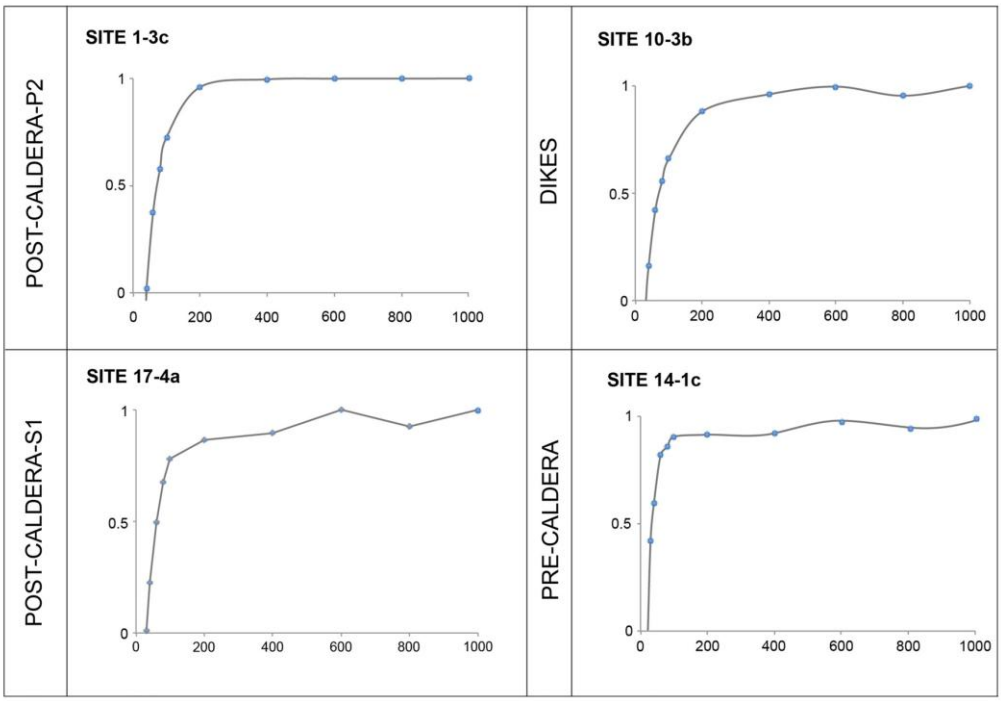

961 **Fig. 4** Acquisition of the remanent magnetization. *X*-axis: normalized remanent
962 magnetization. *Y*-axis: applied magnetic field in milli Tesla. All diagrams show
963 the presence of low coercive ferromagnetic minerals

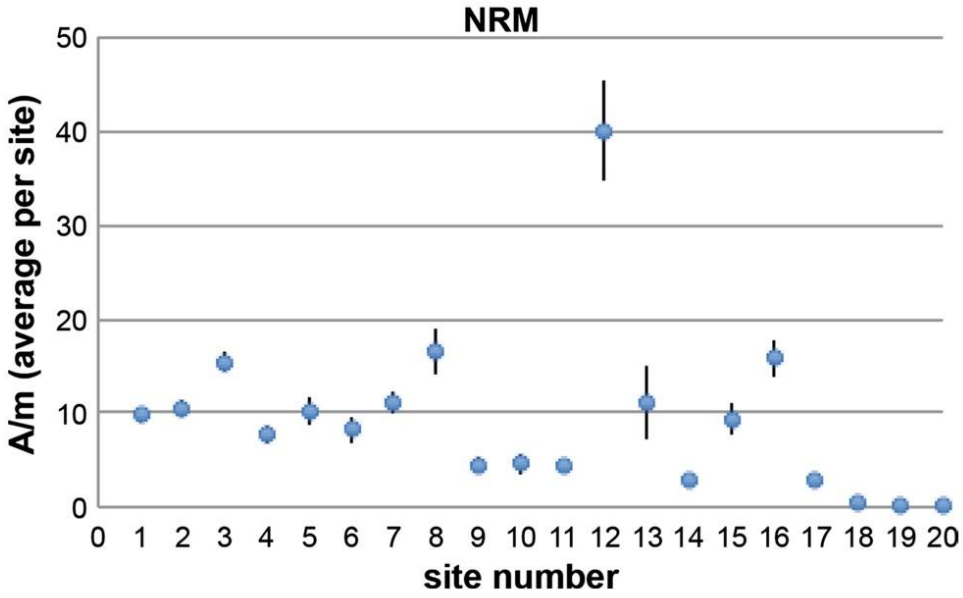

964 **Fig. 5** Mean values of the natural remanent magnetization for every site with the
965 standard deviation. For samples location, see Fig. 2

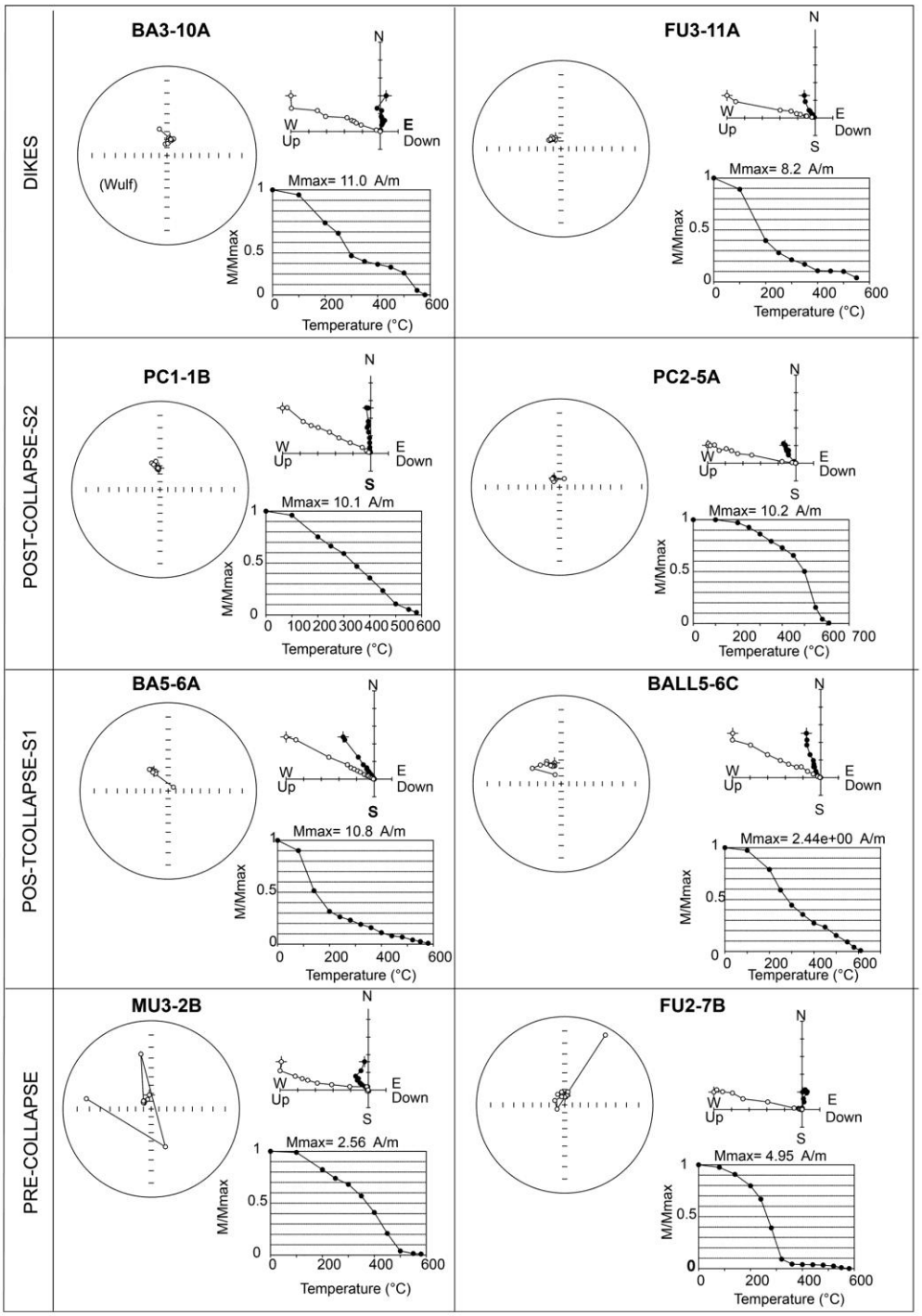

966 **Fig. 6** Selected demagnetization diagrams: orthogonal, stereoplots and decay
967 of remanence during the stepwise demagnetization. In the orthogonal diagrams,
968 *white* (*black*) *dots* are *vertical* (*horizontal*) projection of the magnetic vector. In
969 the stereoplots, *open circles* point to the *upper* hemisphere

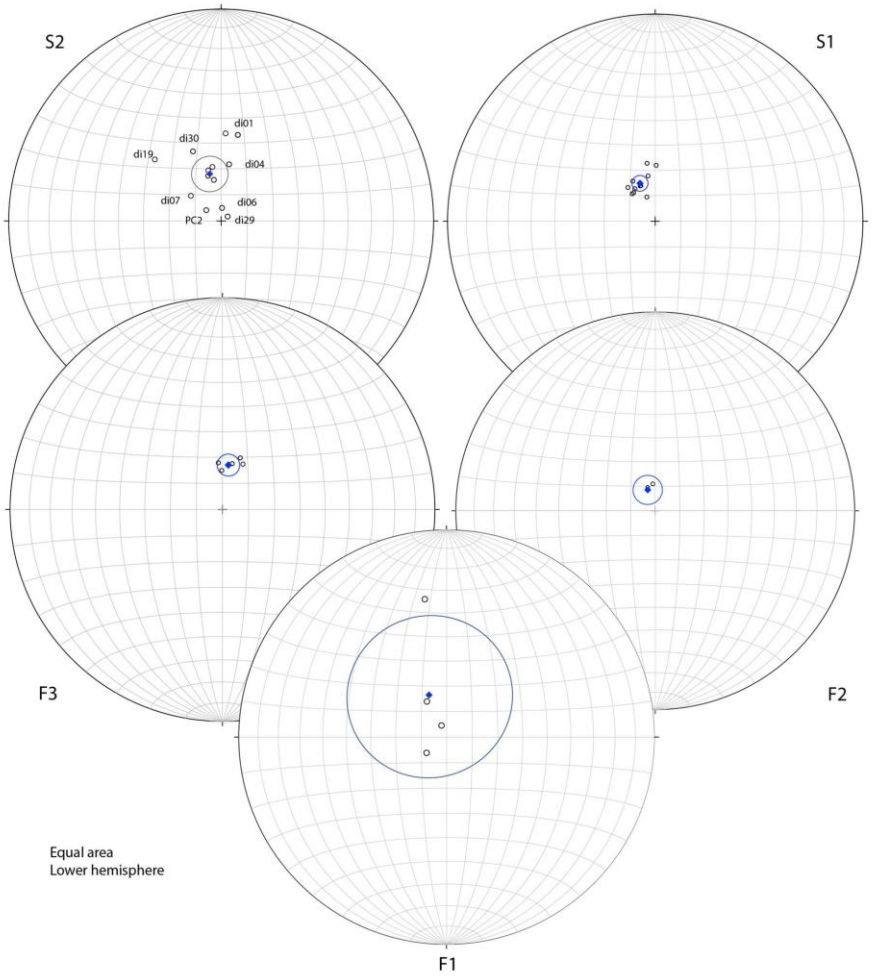

970 **Fig. 7** Stereoplots showing average per site (*white dots*) and average per
971 volcanic unit (*blue dot*, Table 5)

972

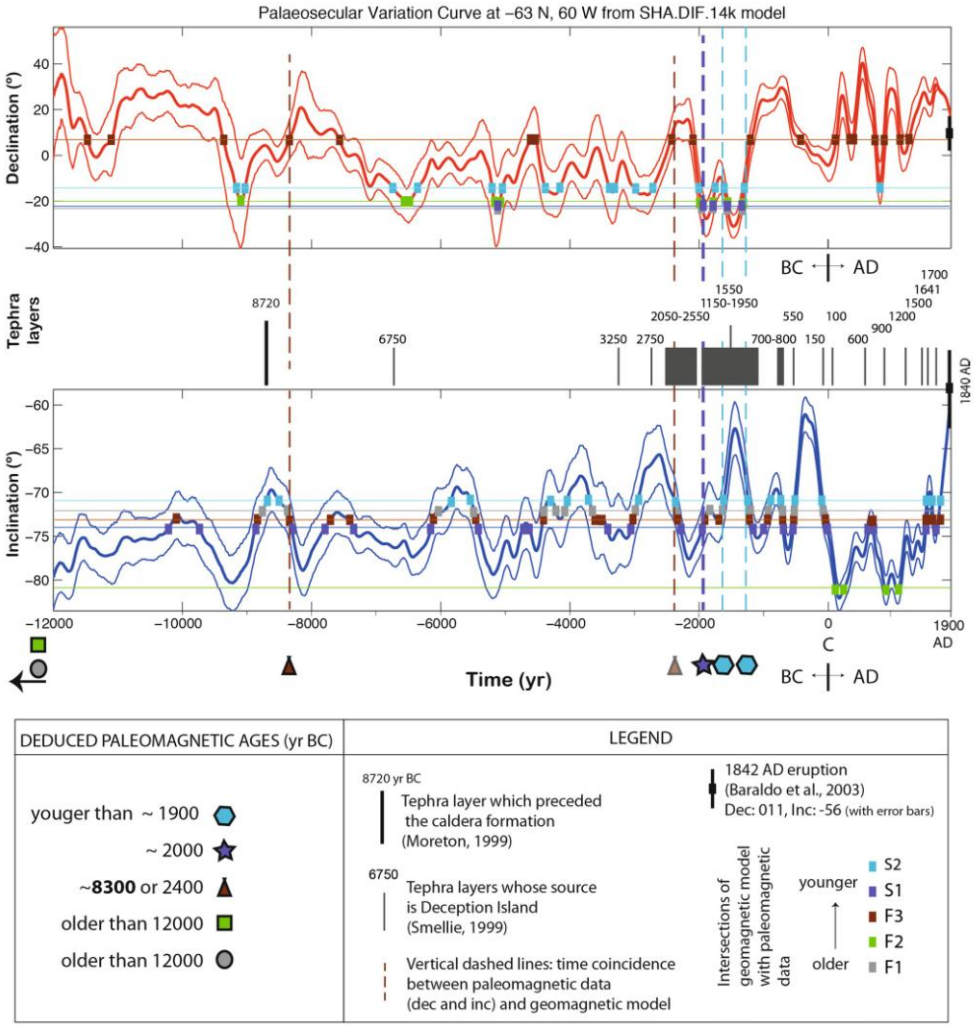

973 **Fig. 8** Probable ages for the volcanic units obtained after comparing
974 paleomagnetic data with the geomagnetic model. When *horizontal color lines*
975 (averaged dec and inc of volcanic units) cross the geomagnetic model average
976 values, a *square mark* is posed. *Vertical dashed lines* mark probable ages
977 obtained when inclination and declination paleomagnetic data (*squares*) overlap
978 at the same time with the geomagnetic model data. Paleomagnetic data of a
979 historic eruption (1842 AD) from Baraldo et al. (2003) are also plotted with *error*
980 *bars* (εINC = α95; εDEC = α95/cos INC). Tephra occurrences are also plotted
981 (Moreton 1999; Smellie 1999)

Site	Map site	UTM coordinates	Relative age	Dike strike	Dike thickness	Dike relationship with the volcanic units
BA3	8	20E 0616568/3014650	Post-caldera—S1	155, 85W	70 cm	Cut Baily Head (S1)
FU3	10	20E 0615529/3015543	Post-caldera—S1	075, 85N	>60 cm	Cut Fumarole Bay Fm (F1)
FU5	11	20E 0615539/3015644	Post-caldera—S1	057,73N	60 cm	Cut Fumarole Bay Fm (F1)
TE1	15	20E 0615902/3019585	Post-caldera—S1	060, 70N	80 cm	Cut F3
BA8	6	20E 0616244/3014146	Post-caldera—S1	145, 80 W	?	Cut F3 (not cut totally)

982 **Table 1** Dike sites. UTM coordinates (WGS84), relative age, attitude, thickness
983 and relationship with other volcanic units. See Fig. 2 for sites location.
984 Lithostratigraphic units are according to Smellie and López-Martínez (2000,
985 2002)

Site	Map site	UTM coordinates	Caldera stages units	Surface orientation	Thickness	Type of deposit	Formation or member
PC1	2	20E 0622024/3012567	Post-caldera—S2	146, 80W	3 m	Lava	Pendulum Cove
PC2	1	20E 0622146/3012547	Post-caldera—S2	137, 30NE	–	Lava	Pendulum Cove
PC3	3	20E 0621507/3012703	Post-caldera—S2	100, 20N	–	Lava	Pendulum Cove
CL1	5	20E 0617933/3013680	Post-caldera—S2	Subhorizontal	–	Scoriaceous lava	Pendulum Cove
BA5	7	20E 0616568/3014650	Post-caldera—S1	140, 15N	–	Lava	Stonethrow Ridge (Kendall Terrace M.)
FU7	13	20E 0615636/3016590	Post-caldera—S1	015, 35E	4 m	Scoriaceous lava	Stonethrow Ridge (Kendall Terrace M.)
FU8	12	20E 0615442/3016593	Post-caldera—S1	015, 25E	4 m	Scoriaceous lava	Stonethrow Ridge (Kendall Terrace M.)
BALL5	17	20E 0622920/3015131	Post-caldera—S1	030, 35E	–	Lava	Stonethrow Ridge (Kendall Terrace M.)
PEN1	16	20E 0622769/3018188	Post-caldera—S1	140, 15SW	–	Lava	Stonethrow Ridge (Kendall Terrace M.)
CO1	4	20E 0620268/3013239	Post-caldera—S1	Subhorizontal	–	Lava	Stonethrow Ridge (Kendall Terrace M.)
MU3	14	20E 0615620/3017911	Pre-caldera—F2	148, 20W	50 m	Lava	Basaltic Shield
FU2	9	20E 0615690/3015279	Pre-caldera—F1c	042, 36NW		Pillow lavas	Fumarole Bay
FU1	18	20E 0615690/3015279	Pre-caldera—F1c	042, 36NW	4 m	Microconglomerate, v. breccia	Fumarole Bay
FU4	19	20E 0615539/3015644	Pre-caldera—F1a	–	–	Volcanic breccia	Fumarole Bay
FU6	20	20E 0615539/3015576	Pre-caldera—F1b	–	–	Volcanic breccia	Fumarole Bay

Table 2 Sites. UTM coordinates (WGS84), relative age, attitude, thickness and type of deposit, name of Formation (and member when known). In brackets, lithostratigraphic units (according to Smellie and López-Martínez 2000)

Site-unit	Map site	n/N	DEC (°) uncorrected	DEC (°) corrected	INC (°)	α_{95} (°)	k	ERROR in DEC (α_{95}/INC) (°)
PC1-S2	2	8/8	359	346	−70	4	170	11.70
PC2-S2	1	8/8	319	306	−83	3	229	24.62
PC3-S2	3	8/8	4	351	−69	5	91	13.95
CL1-S2	5	6/8	16	3	−56	5	148	8.94
BA3 (dike)-S1	8	8/8	4	351	−72	5	103	16.18
FU3 (dike)-S1	10	7/8	334	321	−73	7	67	23.94
FU5 (dike)-S1	11	5/8	336	323	−76	4	307	16.53
TE1 (dike)-S1	15	6/7	354	341	−80	6	97	34.55
BA8 (dike)-S1	6	8/8	5	352	−67	4	142	10.24
BA5-S1	7	6/8	344	331	−72	2	916	6.47
FU7-S1	13	8/8	14	1	−68	3	228	8.01
FU8-S1	12	5/8	333	320	−76	8	79	33.07
BALL5-S1	17	8/8	341	328	−74	4	147	14.51
PEN1-S1	16	8/8	350	337	−75	4	167	15.45
CO1-S1	4	8/8	351	338	−75	3	277	11.59
MU3-F2	14	6/8	325	312	−83	5	164	41.03
FU2-F1	9	8/8	349	336	−85	5	91	57.37
FU1-F1	18	7/7	344	331	−74	8	49	29.02
FU4-F1	19	6/7	245	232	−80	11	15	63.34
FU6-F1	20	7/7	4	351	−33	38	52	45.3

989 **Table 3** Paleomagnetic data from samples taken in 2009 (magnetic declination
990 in 2009 D = 12.76°E, −0.05° change/year corrected in fourth column) See Fig. 2
991 for site location. Lithostratigraphic units are according to Smellie and López-
992 Martínez (2000)

Site	Dec	Inc	Age or unit	Type of deposit
DI01	10.6	−56.1	1842 AD	Lava
DI04	8	−68	S2	Lava
DI03	344	−72	S2	Lava
DI30	338.5	−60.7	S2	Lava
DI29	55.7	−87.4	S2	Lava
DI27	350.1	−73.9	S2	Lava
DI19	312.9	−55	S2	Lava
DI06	4.3	−85.5	S2	Lava
DI07	310.3	−74.8	S2	Strombolian
DI23	358.7	−74.7	F3	Pyroclastic
DI20	11.9	−72.4	F3	Pyroclastic
DI15	355.2	−72.2	F3	Surges
DI12	346.8	−76.3	F3	Surges
DI09	24.3	−70.6	F3	Pyroclastic
DI08	19.3	−69.3	F3	Pyroclastic
DI13	341.7	−79.6	F2	Lava
DI10	355.3	−79.2	F2	Lava

Table 4 Paleomagnetic data from Baraldo et al. (2003) (only sites with α95 < 10°). Lithostratigraphic units are according to Smellie and López-Martínez (2000)

Unit	*N* sites	Mean		Mean			Error in dec (alpha95/cosINC)
		DEC		INC	alpha95	*k*	
S2	13	346	−14	−71	7	34	21.05
S1	11	338	−22	−74	3	198	10.88
F3	6	7	7	−73	4	218	13.68
F2	3	340	−20	−81	6	288	38.35
F1	4	337	−23	−72	32	7	103.55

Table 5 Paleomagnetic data (new and from Baraldo et al. 2003) averaged per lithostratigraphic unit. Lithostratigraphic units are according to Smellie and López-Martínez (2000)